Kinetics of the OH + CH_3CF_2Cl Reaction over an Extended Temperature Range

Tunchen D. Fang[†]

Physical Optics Corporation, 2545 W. 237th Street, Suite B, Torrance, California 90505-5228

Philip H. Taylor*[,‡] **and Barry Dellinger**

Environmental Sciences and Engineering Group, University of Dayton Research Institute, 300 College Park, Dayton, Ohio 45469-0132

Chris J. Ehlers and Rajiv J. Berry[§]

Center for Computational Modeling of Nonstructural Materials, WL/MLBT, Wright-Patterson AFB, Ohio 45433

Received: December 16, 1996; In Final Form: May 12, 1997[⊗]

Rate coefficients of the reaction of hydroxyl (OH) radicals with CH_3CF_2Cl over an extended temperature range are reported. Measurements were performed using a laser photolysis/laser-induced fluorescence technique under slow flow conditions at a total pressure of 740 ± 10 Torr. Arrhenius plots of the data exhibited significant curvature and were fitted to the form of $k(T) = AT^B \exp(-C/T)$. A semiempirical fitting approach was used in which A and B were obtained from transition state theory (TST) and C was determined from a nonlinear least-squares fit to the experimental data. *Ab initio* calculations were used to reveal the thermochemical properties of the activated complex. The resulting modified Arrhenius expression was $k(295-808\ \text{K}) = (1.20 \pm 0.32) \times 10^{-17}\ T^{1.89\pm0.05} \exp[(-1541 \pm 128)/T]\ \text{cm}^3\ \text{molecule}^{-1}\ \text{s}^{-1}$. This semiempirical fit is shown to be superior to a purely empirical fit to the data. The expression was in good agreement with experimental results and previous experimental studies between temperatures of 240 and 480 K. The TST-based modified Arrhenius expression is compared to previous TST and structure−activity relationship predictions.

Introduction

Recognition of the adverse impact of chlorofluorocarbons (CFCs) on stratospheric ozone has prompted an international effort to replace CFCs with environmentally acceptable alternatives.[1−4] Examples include HCFC-22 (CHF_2Cl) as a replacement for CFC-12 in industrial refrigeration units and HCFC-141b (CH_3CFCl_2) as a replacement for CFC-11 in foam-blowing applications. Although the ozone depletion potentials (ODPs) of these compounds are more than a factor of 10 lower than the CFCs they are replacing, their ODPs remain significant when presented in terms of atmospheric lifetimes.[5] As a result, second-generation replacements for these HCFCs are currently under investigation to further minimize the long-term impact on stratospheric ozone depletion.

High-temperature incineration is used as the primary means of disposal of large quantities of HCFCs. To successfully model HCFC combustion, accurate semiempirical Arrhenius parameters describing rate behavior over extended temperature ranges are required. With the exception of our recent studies of HCFC-21 ($CHFCl_2$) and HCFC-22 (CHF_2Cl),[6] previous measurements have only been reported over a narrow low-temperature range encompassing tropospheric and stratospheric conditions.[7] At temperatures above 480 K, the prediction of rate constants for these compounds has been based solely on semiempirical transition state theory (TST)[8,9] and structure−activity relationship (SAR) calculations.[10] Rate coefficient measurements over an extended temperature range are needed to verify and/or refine previously published TST and SAR models.

In this paper, we report high-precision rate coefficients for the reaction of OH with CH_3CF_2Cl (HCFC-142) over an extended range of temperature:

$$CH_3CF_2Cl + {}^{\bullet}OH \rightarrow H_2O + CH_2CF_2Cl \qquad (\Delta H^\circ_{298} = -13.86\ \text{kcal/mol})^{11}$$

Significant curvature was observed in an Arrhenius plot of the data. To provide a more accurate description of the experimental results, conventional TST calculations cast in the form $k(T) = AT^B \exp(-C/T)$ were conducted where both A and B were calculated using TST with C determined from a nonlinear least-squares fit to the experimental data. *Ab initio* calculations were used to define the activated complex. The semiempirical TST calculation is shown to be superior to a purely empirical fit to the data. The modified Arrhenius expression is compared to previous TST and SAR predictions.

Experimental Approach and Data Reduction

The experimental procedures are very similar to our previous studies of OH reactions with chlorinated hydrocarbons and C_1 HCFCs.[6,12−14] As a result, we only briefly summarize the procedures here.

OH radicals are produced by 193.3 nm photodissociation of $HCFC/N_2O/H_2O/He$ gas mixtures with a ArF excimer laser (Questek Model 2860). Initial OH concentrations, $[OH]_0$, ranged from 6×10^9 to 2×10^{10} molecules cm^{-3} and were determined from the measured excimer laser fluence and published values of the N_2O absorption coefficient (8.95×10^{-20} $\text{cm}^2\ \text{molecule}^{-1}$ at 298 K),[15] a photodissociation quantum yield for $O(^1D)$ production of unity,[16] and the rapid reaction of $O(^1D)$

* Corresponding author.
[†] Tel: (310) 530-1416. Fax: (310) 530-4577. E-mail: TDFang@msn.com.
[‡] Tel: (513) 229-3604. Fax: (513) 229-2503. E-mail: Taylorph@udri.udayton.edu.
[§] Tel: (513) 255-2467. Fax: (513) 255-9019. E-mail: Berryrj@ml.wpafb.af.mil.
[⊗] Abstract published in *Advance ACS Abstracts,* July 15, 1997.

S1089-5639(96)04095-9 CCC: $14.00

with H_2O (95% conversion in <20 μs). Experiments were conducted for photolysis laser intensities of 0.3−0.9 mJ cm^{-2}. Following reaction initiation, time-resolved OH profiles were measured as functions of HCFC concentration using laser-induced fluorescence with a pulsed Nd:YAG pumped-dye laser (Quanta Ray Model DCR-2/PDL-2) emitting at the wavelength of 282.1 nm. Broad band fluorescence was collected at 309 nm using a PMT/band-pass filter combination. An increase in sensitivity, due to the addition of Brewster windows to the optical reactor, permitted OH radical decays to be followed over at least three 1/e decay lifetimes.

In order to uniformly control the temperature, four symmetrical ceramic heaters surround the optical reactor adjacent to the reaction zone. The gas temperature was measured with a chromel-alumel thermocouple positioned ~2 mm from the probe intersection volume. Measurements using a second retractable chromel-alumel thermocouple indicated a variation of less than 3 K across the detection volume for gas temperatures ranging from 295 to 1000 K.

All experiments were carried out under slow flow conditions, and the buildup of reaction products was minimized. Individually-controlled gas flows of $CH_3CF_2Cl/N_2O/H_2O/He$ were thoroughly mixed before entering the optical reactor. The composite flow conditioned the reactor for 1−3 min prior to the onset of data collection, thereby minimizing any effects due to reactant adsorption on the reactor walls. Flow rates were controlled with differential flow transducers, and the total volumetric flow rate just downstream of the reactor was measured before and after each experiment with a bubble meter. All experiments were conducted at a total pressure of 740 ± 10 Torr. Stock samples of CH_3CF_2Cl were obtained from PCR, Inc. This relatively unreactive sample was prepared undiluted in a 0.96 L Pyrex vessel at 740 ± 10 Torr and introduced into the gas mixture and delivery system using a calibrated syringe pump (Sage Instruments, 341B). $[CH_3CF_2Cl]_0$ was varied from 1×10^{15} to 1.1×10^{16} molecule cm^{-3}.

Over the entire temperature range, reactive and diffusive OH radical decay profiles exhibited exponential behavior and were fitted by the following nonlinear expression

$$[OH] = [OH]_0 \exp(-k't) + \gamma \qquad (1)$$

where γ is the constant background signal level and t is the time delay between the two lasers. Because $[CH_3CF_2Cl] >$ 1000[OH] in all reactive experiments, exponential OH radical decays of pseudo-first-order decay constant $k' = k[CH_3CF_2Cl] + k_d$ were observed. k_d is the first-order rate constant for OH radical disappearance from the probe volume due to diffusion and reaction with impurities in the carrier gas. The bimolecular rate constant, k, was obtained from the slope of the least-squares straight line through the graph of k' versus $[CH_3CF_2Cl]$, as illustrated in Figure 1.

Gas chromatography−mass spectrometry (GC−MS) analyses indicated that the CH_3CF_2Cl sample was free of contaminants (>99.9% pure). The remaining chemicals used in our gas delivery system had the following stated minimum purities: He (99.999+%); N_2O (99.9%); H_2O (HPLC organic-free reagent grade). The absorption cross section for CH_3CF_2Cl at 193 nm is 5.5×10^{-21} cm^2 $molecule^{-1}$.[17] For a 0.5 mJ/cm^2 laser fluence and a 10 ns pulse width, laser photolysis of the substrate was calculated to be very small (~0.0005%). The effect of laser photolysis on the substrate was observed to be insignificant on the basis of numerous experiments where variation of the excimer laser intensity had no observable effect on OH decays. Previous absorption coefficient measurements with chlorinated hydrocarbons at 193 nm suggested that substrate photolysis may increase with both increasing Cl substitution and increasing temperature.[13] However, no effect was observed for CH_3Cl ($\sigma = 7.5 \times 10^{-20}$ cm^2 $molecule^{-1}$).[17] The effect of a possible increase in CH_3CF_2Cl absorption of the 193 nm photolysis radiation at elevated temperatures on the OH decays is not believed to be significant. This conclusion is based on the combination of low absorption cross section (more than a factor of 10 lower than CH_3Cl) and the very low laser fluences used in these experiments. Cl atom production from the photolysis of CH_3CF_2Cl does not impact the reported measurements due to the much slower rates for H abstraction (4.0×10^{-16} cm^3 $molecule^{-1}$ s^{-1}).[17]

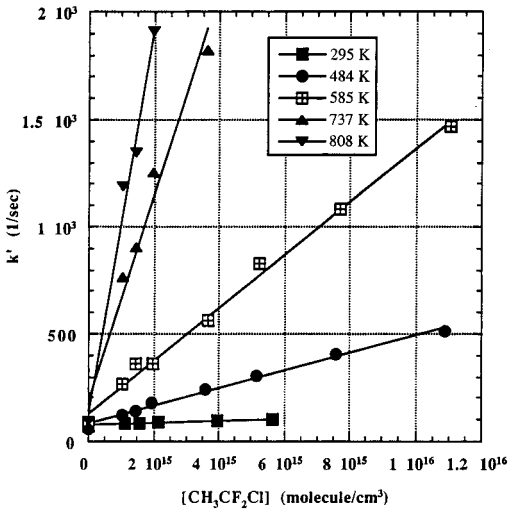

Figure 1. Plot of pseudo-first-order rate coefficient, k', versus $[CH_3CF_2Cl]$ for five reaction temperatures.

TABLE 1: Absolute Rate Coefficients for k_1

temperature (K)	$10^{15} k_1$ (cm^3 $molecule^{-1}$ s^{-1})	temperature (K)	$10^{15} k_1$ (cm^3 $molecule^{-1}$ s^{-1})
295	3.77 ± 0.43[a]	434	31.39 ± 1.53
305	3.96 ± 0.55	459	39.93 ± 2.65
318	4.93 ± 0.43	484	54.99 ± 3.01
329	6.50 ± 0.42	511	70.41 ± 3.21
344	9.65 ± 0.37	545	99.50 ± 3.24
350	7.97 ± 0.79	585	144.30 ± 4.37
359	12.11 ± 0.68	625	198.64 ± 8.24
376	14.52 ± 0.36	676	311.95 ± 19.14
393	19.16 ± 1.27	737	666.80 ± 40.62
400	17.00 ± 1.70	808	922.43 ± 44.49
411	23.47 ± 1.69		

[a] Errors represent $\pm 2\sigma$.

Experimental Results

Absolute rate constants for k_1 are shown in Table 1 and depicted in Arrhenius form in Figure 2. Random error limits ($\pm 2\sigma$) derived from a propagation of error analysis ranged from 6% to 23%. To our knowledge, this is the first report of experimental measurements for these reactions above temperatures of 480 K. Also shown in Figure 2 are previous measurements reported using different techniques.[18−24] With the exception of the nearly 100% larger rate measurements of Clyne and Holt[21] throughout the entire temperature range of their study and the ~30−35% smaller rate measurements of Gierczak et al.[24] at 427, 374, and 297 K, our overlapping rate measurements were in excellent agreement (within ±20%) with previous measurements. The much larger rate measurements of Clyne and Holt[21] infer a systematic error, perhaps related to reactant impurities. A plausible reason for the lower rate measurements of Gierczak et al.[24] is difficult to ascertain given

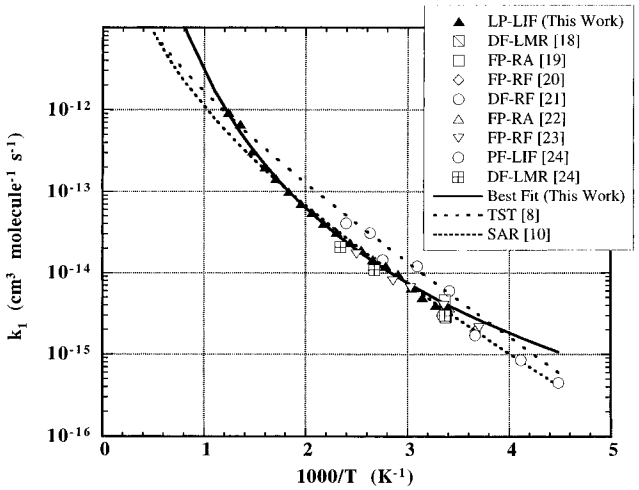

Figure 2. Arrhenius plot of experimental measurements for k_1. Also shown are the results of previous transition state theory (TST)[8] and structure−activity relationship (SAR)[10] calculations.

the demonstrated lack of measurable reactant impurities and the unlikelihood of substrate photolysis.

Rate measurements were observed to rapidly increase at ∼900 K ($k_1 = 2.11 \times 10^{-12}$ cm^3 molecule^{-1} s^{-1} at 895 K). The increase in observed rate coefficient may be attributable to the reaction of OH with HCl[25] and/or CH_2═CF_2, both primary reaction products of the four-center unimolecular decomposition of CH_3CF_2Cl.[26] This effect is primarily due to dramatic increases in concentration of the products (the HCl and/or CH_2═CF_2 concentration increases exponentially with temperature) and not simply differences in relative rates (OH reaction with HCl and CH_2═CF_2 versus CH_3CF_2Cl is actually more favorable at low temperatures). A similar, less dramatic increase in k_1 was evident at 737 K and 808 K (see Figure 2). These measurements were adequately described by transition state theory (TST) calculations (*vide infra*) and were considered representative of k_1. Experimental data at 900 K and higher temperatures were not consistent with TST calculations (a rate coefficient higher by more than a factor of 2) and thus were not considered representative of k_1.

The Arrhenius plot for k_1 demonstrated significant curvature, particularly above 500 K. A nonlinear, least-square fit of our data (weighted as $\omega_k = 1/\sigma_k^2$) to the modified Arrhenius equation $k = AT^B\exp(-C/T)$ produced the following expression (error limits represent $\pm 2\sigma$) denoted as the "best fit" in Figure 2:

$$k_1(295-808\ \mathrm{K}) = 2.05 \pm 17.2 \times 10^{-30}\, T^{6.01\pm1.17} \exp(308 \pm 552/T) \quad (2)$$

The error limits were derived from an iterative χ^2 minimization technique (least squares). The large temperature exponent in eq 2 is indicative of the substantial degree of curvature in the Arrhenius plot. This best fit expression is consistent with available data (excluding Clyne and Holt[21]) between 277 and 670 K but overestimates previous measurements at 243 and 222 K[24] by as much as a factor of 2.

The parameters comprising the modified Arrhenius equation are strongly coupled, and covariance terms are required to assign a meaningful estimate of uncertainty to bimolecular rate constant predictions at higher temperatures. Covariance terms obtained from a weighted Levenberg−Marquardt algorithm were as follows: COV_{AB}, -5.05×10^{-30}; COV_{AC}, -2.37×10^{-27}; COV_{BC}, 160.4. These values translate into an uncertainty (2σ) at 1000 and 2000 K of ±27% and ±118%, respectively.

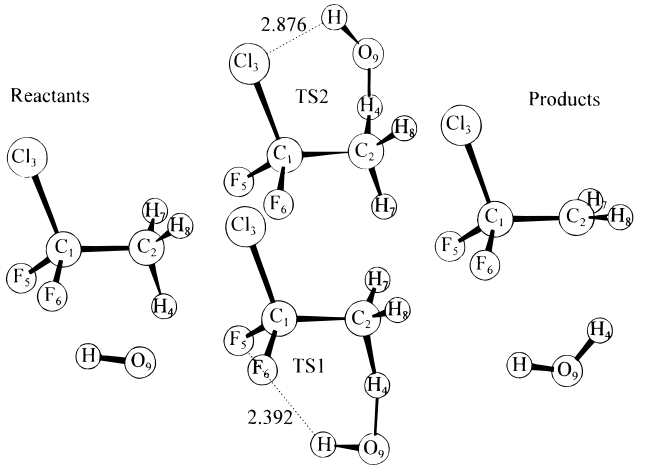

Figure 3. G2(MP2) reaction coordinate for $CH_3CF_2Cl + OH \rightarrow CH_2CF_2Cl + H_2O$. Two transition states are shown.

Development of Semiempirical Arrhenius Parameters

In the absence of experimental data above 480 K, previously reported modified Arrhenius expressions[8] based on curve-fitting approaches were void of true physical meaning. In this section, we report a new methodology to predict the rate coefficient by integrating our experimental measurements over a wider temperature range with conventional transition state theory and *ab initio* calculations.

Although the purely empirical fit is the best statistical representation of the data, we have previously shown that the magnitudes of *A*, *B*, and *C* for these reactions are often theoretically implausible.[6] Consequently, a semiempirical fitting approach that provides physical insight into the thermodynamic properties of the respective transition states has been used. Our approach was to calculate *A* and *B* using conventional TST and then determine *C* by an empirical fit to the three-parameter expression that has now been reduced to one variable. This approach was first demonstrated by Shaw[27] and Cohen[28,29] in TST calculations for the reactions of O atoms and OH radicals with alkanes and halogenated alkanes.

This approach was justified because *A* and *B* can be expressed in terms of the thermodynamic quantities $\Delta C_p^{\ddagger}$ and $\Delta S_p^{\ddagger}$, which are relatively accurately calculable using TST (whereas *C* is related to $\Delta H_p^{\ddagger}$, which is not accurately calculable using TST). Following Shaw,[27] we can show

$$A = (R'k/h)298(-\Delta C_{p\ T}^{\ddagger}/R)\exp[(\Delta S_{p\ 298\mathrm{K}}^{\ddagger} - \Delta C_{p\ T}^{\ddagger})/R] \quad (3)$$

$$B = 2 + (\Delta C_{p\ T}^{\ddagger})/R \quad (4)$$

$$C = (\Delta H_{p\ 298\mathrm{K}}^{\ddagger} - 298\Delta C_{p\ T}^{\ddagger})/R \quad (5)$$

where $\Delta S_{p\ 298\mathrm{K}}^{\ddagger}$ is the entropy of the transition state at 298 K in pressure standard state; $\Delta C_{p\ T}^{\ddagger}$ is the heat capacity of the transition state at a specified temperature, $\Delta H_{p\ 298\mathrm{K}}^{\ddagger}$ is the enthalpy of the transition state at 298 K in pressure standard state, *R* is the ideal gas constant in cal/mol K units, *R*′ is the ideal gas constant in (L atm)/mol K units, *k* is the Boltzmann constant, and *h* is Planck's constant. The units of *A* are the same as those of $k(T)$, i.e. L/(mol s).

$\Delta S_{p\ 298\mathrm{K}}^{\ddagger}$ was previously calculated by Cohen and Benson[8] using the haloalkane reagent as the reference compound. They then reported a modified Arrhenius expression over a wide temperature range by combining TST calculations and curve-

TABLE 2: *Ab Initio* Optimized Geometries[a] and Ground State Relative Energies[b] for $CH_3CF_2Cl + OH \rightarrow CH_2CF_2Cl + H_2O$

parameter	reactants	TS1[c]	TS2[d]	products
bond lengths				
C1−C2	1.499(1.504)	1.491(1.495)	1.494(1.499)	1.471(1.479)
C1−Cl3	1.775(1.775)	1.773(1.775)	1.778(1.775)	1.791(1.787)
C1−F5	1.358(1.328)	1.365(1.331)	1.353(1.324)	1.356(1.326)
C1−F6	1.358(1.328)	1.352(1.324)	1.358(1.329)	1.356(1.326)
C2···H4	1.092(1.083)	1.242(1.330)	1.243(1.331)	
C2−H7	1.090(1.081)	1.087(1.077)	1.090(1.080)	1.080(1.072)
C2−H8	1.090(1.081)	1.088(1.077)	1.087(1.077)	1.080(1.072)
H4···O9		1.241(1.177)	1.231(1.172)	0.969(0.947)
O9−H	0.979(0.958)	0.979(0.955)	0.979(0.955)	0.969(0.947)
valence angles				
C2−C1−Cl3	112.7(112.6)	112.4(111.9)	112.5(112.5)	111.7(111.8)
C2−C1−F5	110.4(110.6)	110.1(110.4)	110.7(110.9)	111.2(111.2)
C2−C1−F6	110.4(110.6)	110.9(111.1)	110.2(110.2)	111.2(111.2)
C1−C2−H4	110.0(110.0)	105.2(105.6)	108.8(108.9)	
C1−C2−H7	107.7(107.9)	112.6(113.4)	110.4(111.5)	118.6(118.3)
C1−C2−H8	110.0(110.0)	112.5(113.4)	112.8(113.6)	118.6(118.3)
C2−H4−O9		163.1(172.0)	169.0(175.9)	
H4−O9−H		99.7(100.9)	100.3(101.1)	104.0(105.5)
dihedral angles				
F5−C1−C2−Cl3	121.0(120.8)	120.3(120.4)	121.2(121.2)	120.0(120.1)
F6−C1−C2−Cl3	−121.0(−120.8)	−121.6(−121.0)	−120.4(−120.3)	−120.0(−120.1)
Cl3−C1−C2−H4	−60.5(−60.5)	−176.9(−176.3)	−61.4(−61.3)	
Cl3−C1−C2−H7	180.0(180.0)	−61.0(−62.0)	−175.3(−173.9)	−81.7(−81.1)
Cl3−C1−C2−H8	60.5(60.5)	68.6(70.4)	57.1(55.7)	81.7(81.1)
C1−C2−H4−O9		43.4(47.0)	57.1(68.7)	
C2−H4−O9−H		−6.6(−10.0)	−13.8(−25.8)	
relative energies				
HF/6-31G(d)	0.0	29.95	31.00	3.61
MP2/6-31G(d)	0.0	10.99	12.09	−8.44
G2(MP2)	0.0	5.11	5.50	−13.91

[a] Result of MP2/6-31G(d) (HF/6-31G(d) in parentheses) optimization. Bond lengths in angstroms and angles in degrees. See illustration in Figure 3 for atom label definition. [b] Ground state energies in kcal/mol relative to the combined energy of the reactants. [c] Conformation with OH directed toward fluorine. [d] Conformation with OH directed toward chlorine.

fitting schemes to the available low-temperature experimental measurements. We have utilized the same general approach; however, we used *ab initio* calculations to provide a more accurate definition of the transition state geometry.

The *ab initio* calculations were performed using the GAUSSIAN code[31,32] on Cray Y-MP, Cray C-90, HP-PARisk, and SGI Power-Challenge computers. First, the geometries of the reactants, transition state (TS), and products were optimized at the HF and MP2(FU) levels using the 6-31G(d) atomic basis set. Vibrational frequencies for the optimized structures were computed to evaluate the zero-point energies as well as to confirm the location of minima (no imaginary frequency) or TS (one imaginary frequency only). Single-point energy evaluations at the MP2 optimized geometries were used to obtain the G2(MP2) energy as proposed by Curtiss *et al.*[33] The G2(MP2) energies for the reactants, products, and transition state were computed by including the zero-point energies calculated at the HF level (using frequencies scaled by 0.8929).

Two stable TS conformations were identified for this reaction (cf. Figure 3): a conformation with OH directed toward the F atom (TS1) and one where the OH is directed toward the Cl atom (TS2). The ground state energies of the transition states and products relative to the combined energy of the reactants are listed in Table 2. All three levels of theory (i.e. the HF/6-31G(d), MP2/6-31G(d) and G2(MP2) levels) predict TS1 to be slightly more stable (by 1.05, 1.10, and 0.38 kcal/mol, respectively) than TS2. The reaction is computed to be increasingly more exothermic as one progresses from the modest HF/6-31G(d) level to the higher level G2(MP2) method. The G2(MP2) reaction enthalpy of −13.91 kcal/mol (Table 2) is in good agreement with the reported BAC-MP4 value of −13.86 kcal/mol.[11]

Also shown in Table 2, the HF and MP2 geometries agree to within 0.03 Å for bonds and 2° for angles, with the exception of some of the parameters associated with the proton transfer in the TSs. Changes in the $C_2\cdots H_4$ and $H_4\cdots O_9$ distances reveal that the MP2 geometry for TS1 is more reactant-like (tight TS) while the HF geometry is closer to the midpoint of the reactants and products. Scaled frequencies and qualitative assignments for the reactants, TS1, and products are presented in Table 3 and compared with the experimental frequencies reported for CH_3CF_2Cl.[30]

Of the various corrections to the haloalkane model compound, ΔS_{ir} was the largest and most difficult to estimate. Two new internal rotation axes along the C···H and H···O bonds were considered in this calculation. In our previous calculation for CHF_2Cl and $CHFCl_2$,[6] we assumed the barriers to rotation about the C···H and H···O bonds were 1 and 2 kcal/mol, respectively. For the TS of CH_3CF_2Cl, the potential energy surface (PES) was scanned at the HF/6-31G(d) level in order to estimate the internal rotation barriers. For this scan, the $C_2\cdots H_4$ and $C_2\cdots O_9$ distances were held fixed at the HF/6-31G(d) optimized values for the TS1 listed in Table 2. The OH rotor was scanned by varying the $C_1C_2\cdots O_9H$ dihedral from −180° to 180° at 15° intervals, while the CF_2Cl rotor was scanned by varying $Cl_3C_1\cdots C_2H_7$ from −60° to 120° at 15° intervals. The computed PES was used to estimate the barrier for the conversion of TS1 to TS2, i.e., the CF_2Cl rotational barrier (3.6 kcal/mol) and the OH rotational barrier (1.3 kcal/mol). The $C_2\cdots H_4$ rotor was treated as a free rotor.

The Hartree−Fock and MP2 levels of theory (hindered rotor[8] model, TS1 conformation) resulted in values of $\Delta S_{p^{\ddagger}298K}$ of −25.83 and −26.34 cal mol^{-1} K^{-1}, respectively. These values are slightly smaller than the earlier calculations of Cohen and

TABLE 3: *Ab Initio* Vibrational Frequencies Computed at the Stationary Points for $CH_3CF_2Cl + OH \rightarrow CH_2CF_2Cl + H_2O$

	reactants				
assignment	exptl[a]	sym	calc	TS1	products
C−C torsion	272	A″	271 (244)	64 (57)	214 (190)
				106 (79)	
				209 (138)	
C−Cl bend	305	A′	302 (293)	251 (240)	282 (276)
CF2 twist	334	A″	332 (326)	326 (319)	338 (334)
				377 (383)	
				418 (411)	420 (414)
CF2 rock	426	A″	422 (413)	427 (429)	424 (415)
C−Cl str.	438	A′	429 (422)	524 (518)	524 (520)
CF2 wag	543	A′	525 (521)	642 (543)	576 (536)
C−Cl str.	683	A′	675 (661)	714 (652)	721 (705)
CF2 str.	904	A′	914 (903)		
CH3 rock	967	A″	984 (983)		947 (939)
CH3 rock	1134	A′	1151 (1124)	851 (803)	961 (948)
C−C str.	1230	A′	1230 (1231)	944 (921)	1229 (1239)
C··H··O bend				974 (969)	
				1113 (1055)	
CF2 asym. str.	1202	A″	1245 (1235)	1198 (1144)	
				1250 (1236)	1270 (1245)
CH3 umb.	1395	A′	1429 (1413)	1269 (1252)	
CH3 def.	1447	A′	1488 (1450)	1456 (1422)	1455 (1415)
CH3 def.	1447	A″	1490 (1451)		
HOH bend				1505 (1449)	1674 (1630)
CH3 sym. str.	2965	A′	3029 (2895)	3085 (2960)	3155 (3000)
CH3 sym. str.	3035	A′	3126 (2968)	3176 (3041)	3280 (3109)
CH3 asym. str.	3035	A′	3139 (2983)		
OH str.			3608 (3569)	3598 (3602)	3642 (3635)
					3779 (3740)
rxn. coord.				2341i (2926i)	

[a] Assignments and frequencies taken from ref 30.

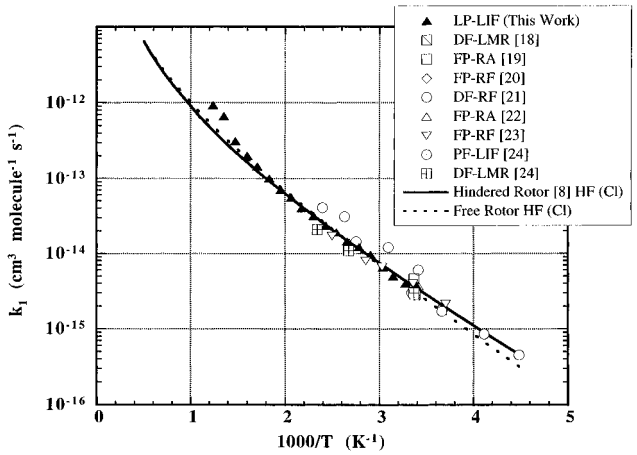

Figure 4. Arrhenius plot of experimental measurements for k_1. Also shown are two transition state theory (TST) calculations using the Hartree−Fock (HF) *ab initio* calculations in conjunction with a hindered rotor[8] and free rotor models. (Cl) refers to the TS conformation (see Figure 3). The value of C in the equation $k = AT^B \exp(-C/T)$ was calculated by minimizing the root mean square deviation of the data set indicated in parentheses.

Benson[8] and Cohen[9] (−24.3 and −25.9 cal mol^{-1} K^{-1}, respectively). To evaluate the temperature exponent, we directly calculated an average $\Delta C_p^{\ddagger}{}_T$ from 298 to 1000 K using the harmonic oscillator−rigid free rotor approximation with a correction for hindered internal rotation in the TS. The details of these calculations were given previously.[6] The resulting mean $\Delta C_p^{\ddagger}{}_T$ was $-0.13R$ and $-0.08R$ for Hartree−Fock and MP2 levels of theory, respectively.

Figures 4−6 present the results of an analysis of the effects of (1) free versus hindered internal rotors (Cohen and Benson[8] model); (2) two different hindered internal rotor models (Cohen and Benson[8] versus the *ab initio* based model); (3) TST

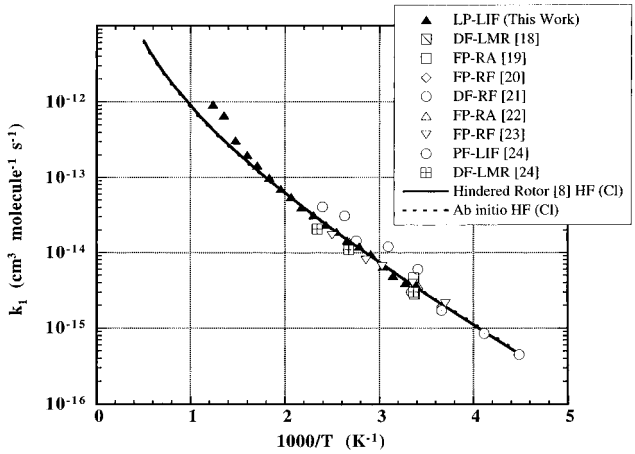

Figure 5. Arrhenius plot of experimental measurements for k_1. Also shown are two transition state theory (TST) calculations using the Hartree-Fock (HF) *ab initio* calculations in conjunction with a hindered rotor model[8] and barriers to rotation based solely on the *ab initio* calculations. (Cl) refers to the TS conformation (see Figure 3). The value of C in the equation $k = AT^B \exp(-C/T)$ was calculated by minimizing the room mean square deviation of the data set indicated in parentheses.

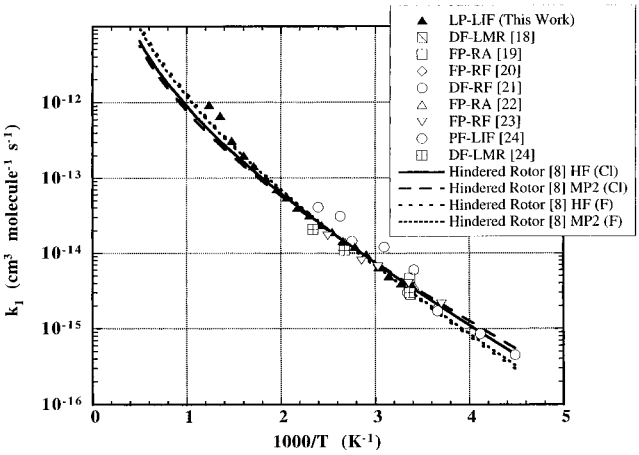

Figure 6. Arrhenius plot of experimental measurements for k_1. Also shown are various transition state theory (TST) calculations using the Hartree−Fock (HF) and MP2 *ab initio* calculations in conjunction with a hindered rotor model.[8] The effect of the two different transition states [(F) refers to the TS1 conformation and (Cl) refers to the TS2 conformation, cf. Figure 3] is also shown. The value of C in the equation $k = AT^B \exp(-C/T)$ was calculated by minimizing the room mean square deviation of the data set indicated in parentheses.

predictions using the Hartree−Fock and MP2 levels of *ab initio* theory; (4) TST predictions for both TS configurations (see Figure 3) using the Hartree−Fock and MP2 levels of *ab initio* theory and the entire experimental data set (excluding only the measurements of Clyne and Holt[21]). As illustrated in Figure 4, similar predictions were obtained for the free internal rotor and hindered internal rotor models above 295 K. As expected, the hindered internal rotor model provided a better description at lower temperatures. No significant deviation was observed between the Cohen and Benson[8] and *ab initio* based hindered internal rotor models (see Figure 5). Despite the measurable difference in the internal rotation barriers estimated by Cohen and Benson[8] and our computed *ab initio* values, the lack of a discernible difference in the TST plots (cf. Figure 5) over an extended temperature range indicated a fortuitous cancellation of errors. Similar predictions were obtained for both the Hartree−Fock and MP2 levels of *ab initio* theory (see Figure 6). A slight deviation was observed between the two TST conformations (TS1 vs TS2). TST calculations using the TS2

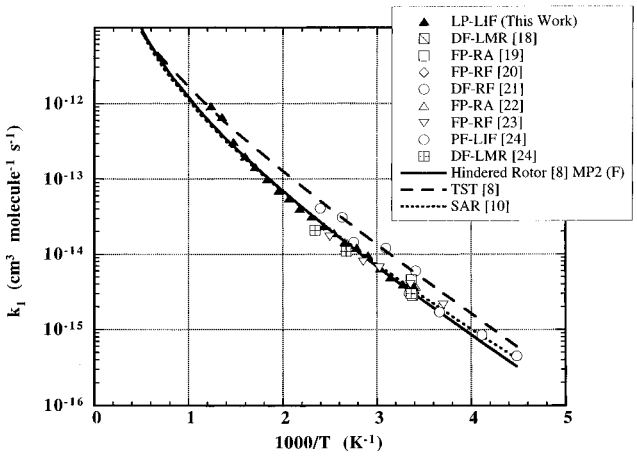

Figure 7. Arrhenius plot of experimental measurements for k_1. Also shown are transition state theory (TST) calculations, *ab initio* calculations (MP2), and previous TST[8] and structure−activity relationship (SAR)[10] calculations.

conformation resulted in a slightly improved fit to the extreme low-temperature data (<295 K), while TST calculations using the TS1 conformation resulted in a slightly improved fit to the higher temperature data (>500 K).

The best fit, TST-based modified Arrhenius expression, as determined from a minimization of nonlinear least-squares error, χ^2, was observed to be the MP2 *ab initio* model (TS1 conformation) combined with the Cohen and Benson hindered rotor[8] model and is given by the following expression:

$$k(295-808\ \mathrm{K}) = (1.20 \pm 0.32) \times 10^{-17}\, T^{1.89\pm0.05} \exp[(-1541 \pm 128)/T]\ \mathrm{cm^3\,molecule^{-1}\,s^{-1}}$$

The uncertainty ($\pm 2\sigma$) in the modified Arrhenius parameters is based primarily on a ±10% uncertainty in the vibrational frequencies as discussed in detail in reference 6. In Figure 7, the best-fit TST-based modified Arrhenius expression is plotted, along with all of the available experimental data, from stratospheric to near-combustion temperatures. The TST-based expression accurately describes all of the available data within an uncertainty of ±25%. The TST expression is thus recommended for use in kinetic modeling of the combustion and atmospheric reactions of CH_3CF_2Cl.

Comparisons of our TST expression with previous TST and SAR calculations are also shown in Figure 7. Good agreement was observed between our TST expression and the SAR calculations. The TST calculation of Cohen and Benson[8] indicates ∼30−50% larger rate coefficients from 200−500 K with the deviation decreasing at higher temperatures (>1000 K).

Implications

There are two implications resulting from this work. The first involves the observation of non-Arrhenius behavior for the reactions of OH radicals with CH_3CF_2Cl. We have also recently reported non-Arrhenius behavior for the reactions of OH radicals with CHF_2Cl and $CHFCl_2$.[6] The significance here is the error that results from use of the simple Arrhenius equation as compared to non-Arrhenius expressions to predict the rate of these reactions at combustion temperatures. For example, the JPL evaluation[17] prediction (which appropriately recommends the simple Arrhenius expression for atmospheric modeling purposes), as compared to the three-parameter expression derived from this study, results in about a factor of 5 underestimation of the reaction rate at 1000 K. This error increases to nearly a factor of 15 at 2000 K.

A second implication involves the ability of conventional TST to reasonably predict the experimental data obtained over a substantial temperature range. The major uncertainty in this approach has previously involved the accurate definition of the transition state geometry and frequencies for each reaction. As shown here, extended temperature measurements and *ab initio* calculations in conjunction with conventional TST provide a framework for improving the accuracy of these predictions. TST calculations that incorporate tunneling and energies computed at higher levels of *ab initio* theory are underway.

Acknowledgment. T.F., P.T., and B.D. acknowledge support from the Environmental Protection Agency (Grant R819861-01-0). C.E. and R.B. acknowledge the Air Force Office of Scientific Research and the Materials Directorate at Wright Laboratory for financial support and computational resources. The authors acknowledge the constructive criticisms of the two reviewers.

References and Notes

(1) Molina, M. J.; Rowland, F. S. *Nature* **1974**, *249*, 810.
(2) Farman, J. D.; Gardiner, B. G.; Shanklin, J. D. *Nature* **1985**, *315*, 207.
(3) Solomon, S. *Nature*, **1990** *347*, 6291 and references therein.
(4) World Meteorological Organization. Global Ozone Research and Monitoring Project. *Scientific Assessment of Stratospheric Ozone*; Geneva, Switzerland, 1989 Vols. I and II, Report No. 20.
(5) Wallington, T. J.; Schneider, W. F.; Worsnop, D. R.; Nielsen, O. J.; Sehested, J.; Debruyn, W. J.; Shorter, J. A. *Environ. Sci. Technol.* **1994**, *28*, 320A.
(6) Fang, T. D.; Taylor, P. H.; Dellinger, B. *J. Phys. Chem.* **1996**, *100*, 4048.
(7) Atkinson, R. *J. Phys. Chem. Ref. Data* **1989**, Monograph 1.
(8) Cohen, N.; Benson, S. W. *J. Phys. Chem.* **1987**, *91*, 162.
(9) Cohen, N. Transition State Theory Calculations for Reactions of OH Radicals with Selected Halogenated Alkanes. Aerospace Report No. ATR-94(8446)-1; The Aerospace Corporation: El Segundo, CA, 1994.
(10) Atkinson, R. *Int. J. Chem. Kinet.* **1986**, *18*, 555.
(11) Melius, C. F. BAC-MP4 Calculation Heats of Formation and Free Energies. Sandia National Laboratories: Livermore, CA, April, 1993.
(12) Jiang, Z.; Dellinger, B.; Taylor, P. H. *J. Phys. Chem.* **1992**, *96*, 8961.
(13) Jiang, Z.; Dellinger, B.; Taylor, P. H. *Int. J. Chem. Kinet.* **1993**, *25*, 9.
(14) Jiang, Z.; Taylor, P. H.; Dellinger, B. *J. Phys. Chem.* **1993**, *97*, 5050.
(15) Selwyb, G.; Podolske, J.; Johnston, H. S. *Geophys. Res. Lett.* **1977**, *4*, 427.
(16) Simonaitis, R.; Heicklen, J. *J. Phys. Chem.* **1973**, *77*, 1932.
(17) DeMore, W. B.; Sander, S. P.; Golden, D. M.; Hampson, R. F.; Kurylo, M. J.; Howard, C. J.; Ravishankara, A. R.; Kolb, C. E.; Molina, M. J. Chemical Kinetics and Photochemical Data for Use in Stratospheric Modeling. JPL Publication 94-26; Jet Propulsion Laboratory, California Institute of Technology: Pasadena, CA, 1994.
(18) Howard, C. J.; Evenson, K. M. *J. Chem. Phys.* **1976**, *64*, 4303.
(19) Paraskevopoulos, G.; Singleton, D. L.; Irwin, R. S. *J. Phys. Chem.* **1981**, *85*, 561.
(20) Watson, R. T.; Machado, G.; Conaway, B.; Wagner, S.; Davis, D. D. *J. Phys. Chem.* **1977**, *81*, 256.
(21) Clyne, M. A. A.; Holt, P. M. *J. Chem. Soc., Faraday Trans.* **1979**, *275*, 582.
(22) Handwerk, V.; Zellner, R. *Ber. Bunsen-Ges Phys. Chem.* **1978**, *82*, 1161.
(23) Liu, R.; Huie, R. E.; Kurylo, M. J. *J. Phys. Chem.* **1990**, *94*, 3247.
(24) Gierczak, T.; Talukdar, R.; Vaghjiana, G. L.; Lovejoy, E. R.; Ravishankara, R. *J. Geophys. Res.* **1991**, *96*, 5001.
(25) Husain, D.; Plane, J. M. C.; Xiang, C. C. *J. Chem. Soc., Faraday. Trans. 2* **1984**, *80*, 713.
(26) Edwards, J. W.; Small, P. A. *Nature* **1964**, *202*, 1329.
(27) Shaw, R. *J. Phys. Chem. Ref. Data* **1978**, *7*, 1179.
(28) Cohen, N. *Int. J. Chem. Kinet.* **1982**, *14*, 1339; **1983**, *15*, 503.
(29) Cohen, N. *Int. J. Chem. Kinet.* **1986**, *18*, 99.
(30) Paddison, S. J.; Chen, Y.; Tschuikow-Roux, E. *Can. J. Chem.* **1994**, *72*, 561.

(31) Frisch, M. J.; Trucks, G. W.; Head-Gordon, M.; Gill, P. M. W.; Wong, M. W.; Foresman, J. B.; Johnson, B. G.; Schlegel, H. B.; Robb, M. A.; Replogle, E. S.; Gomperts, R.; Andres, J. L.; Raghavachari, K.; Binkley, J. S.; Gonzalez, C.; Martin, R. L.; Fox, D. J.; Defrees, D. J.; Baker, J.; Stewart, J. J.P.; Pople, J. A. *Gaussian 92*, Revision F4; Gaussian, Inc.: Pittsburgh, PA, 1992.

(32) Frisch, M. J.; Trucks, G. W.; Schlegel, H. B.; Gill, P. M. W.; Johnson, B. G.; Robb, M. A.; Cheeseman, J. R.; Keith, T. A.; Petersson, G.A.; Montgomery, J. A.; Raghavachari, K.; Al-Laham, M. A.; Zakrzewski, V. G.; Ortiz, J. V.; Foresman, J. B.; Cioslowski, J.; Stefanov, B. B.; Nanayakkara, A.; Challacombe, M.; Peng, C. Y.; Ayala, P. Y.; Chen, W.; Wong, M. W.; Andres, J. L.; Replogle, E. S.; Gomperts, R.; Martin, R. L.; Fox, D. J.; Binkley, J. S.; Defrees, D. J.; Baker, J.; Stewart, J. P.; Head-Gordon, M.; Gonzalez, C.; Pople, J. A. *Gaussian 92*, Revision F4; Gaussian, Inc.: Pittsburgh, PA 1995.

(33) Curtiss, L. A.; Raghavachari, K.; Pople, J. A. *J. Chem. Phys.* **1993**, *98*, 1293.